

# Characterizing the Nonlinear Propagation of Femtosecond Pulses in Bulk Media

Scott A. Diddams, Hilary K. Eaton, Alex A. Zozulya, and Tracy S. Clement, *Member, IEEE*

**Abstract**—Frequency-resolved optical gating is used to characterize the amplitude and phase of intense femtosecond pulses propagating in nonlinear dispersive media. The combined effects of group velocity dispersion (GVD) and third-order nonlinearity ( $n_2$ ) lead to rapid broadening and splitting of the pulses. We present measurements at 800 and 1200 nm and investigate the influence of the chirp of the input field. Measurements are compared with the predictions of one- and three-dimensional nonlinear Schrödinger equations. The influence of the Raman contribution to the nonlinear index of refraction is also examined theoretically.

**Index Terms**—Nonlinear optics, optical propagation in nonlinear media, optical pulse measurements, ultrafast optics.

## I. INTRODUCTION

THE PROPAGATION of intense femtosecond pulses is a field rich in linear and nonlinear phenomena. Peak powers greater than 10 GW, which are readily attained with current laser systems, turn most any medium into an interesting nonlinear sample. In addition, as pulsewidths continue to decrease, the corresponding increase in bandwidth makes linear dispersion even more of an issue. Along with such intense femtosecond pulses have come many challenging problems. Examples include the pulse generation and amplification itself [1], atmospheric propagation [2]–[4], optical communications [5], and laser–plasma interactions [6]. It can be argued that, in all of these cases, accurate information about the complete electric field on a femtosecond time scale would be a powerful tool in understanding the complex light–matter interactions involved. Unfortunately, obtaining this information can be a daunting task. Not only is the short time scale difficult to deal with, but the fields may vary greatly both spectrally and spatially as a function of time.

The nonlinear Schrödinger equation (NLSE) [7] is often used to model the propagation of intense ultrashort pulses in both one and three dimensions, accounting for an instantaneous Kerr nonlinearity, dispersion and diffraction. However, as peak powers increase and spot sizes decrease many of the details

surrounding the propagation of the femtosecond field become unknown. Examples include continuum generation [8], self-trapping [3], [4], and optically induced breakdown [2], [9]. In this regime, the standard NLSE begins to fail. Higher order effects, such as Raman scattering, ionization, and third-order dispersion can be included phenomenologically. But other effects, such as nonparaxiality [10] and shock terms [11] require modification of the assumptions used in deriving the NLSE. Which effects are most important and how they should be modeled are open questions. Furthermore, most experimental data that have thus far been compared with the theories are incomplete in the sense that they only provide details on one aspect of the electric field (usually the spectral intensity). In this paper, we attempt to address some of these issues with measurements of the complete amplitude and phase of intense femtosecond pulses propagating in fused silica. We first present measurements in a regime that can be modeled by the one-dimensional (1-D) NLSE. In this way, we are able to test the technique of frequency-resolved optical gating (FROG) [12], [13] as a tool for tracking nonlinear propagation. We then apply FROG to the analysis of the more complex situation where the three-dimensional (3-D) NLSE can be applied. In this regime the combined effects of diffraction, normal dispersion, and cubic nonlinearity lead to strong self-focusing and pulse splitting. We present measurements of pulse splitting and examine its dependence on the chirp of the input pulse. In addition, we show measurements of the spatial profile of the pulse as it undergoes splitting, and compare these measurements with theoretical calculations. Finally, we include theoretical studies that examine the noninstantaneous (Raman) contribution to the nonlinear index of refraction and its role in the pulse splitting process.

## II. 1-D PROPAGATION

Fused silica is usually the transmissive material of choice in femtosecond laser systems operating in the visible and near infrared because it has low dispersion and is therefore presumed to contribute little to the broadening of femtosecond pulses. However, this may not be the case when intensities greater than  $\sim 1$  GW/cm<sup>2</sup> are present. At these intensities the effect of the nonlinear contribution to the index of refraction becomes important. Furthermore, the interplay between the nonlinearity and the linear dispersion can lead to surprisingly large changes in the pulsewidth over relatively small propagation lengths. In this section, we report results which illustrate this pulse broadening effect.

Manuscript received October 3, 1997; revised February 17, 1998. This work was supported by the National Science Foundation and by the National Institute of Standards and Technology.

S. A. Diddams and H. K. Eaton are with JILA, University of Colorado, Boulder, CO 80309-0440 USA.

A. A. Zozulya was with JILA, University of Colorado. He is currently with the Department of Physics, WPI, Worcester, MA 01609-2280 USA.

T. S. Clement is with JILA, National Institute of Standards and Technology, Boulder, CO 80309-0440 USA.

Publisher Item Identifier S 1077-260X(98)03762-9.

These experiments employ the output of a Ti:sapphire-based chirped pulse amplifier operating at 1-kHz repetition rate. The output of the compressor is collimated in a near-Gaussian beam characterized by a radius of  $w_o = 2.9$  mm ( $1/e^2$  radius of the intensity). The measured average pulse energy is  $795 \mu\text{J}$ , and pulsewidths are sub-100 fs. The pulse train from the compressor is characterized (before and after propagation through fused silica samples of different thickness) using the second-harmonic form of frequency-resolved optical gating (SHG-FROG) [14]. The SHG-FROG measurement is a spectrally resolved noncolinear autocorrelation performed in a  $100\text{-}\mu\text{m}$  piece of BBO. The measurement yields a two-dimensional (2-D) spectrogram from which the amplitude and phase of the electric field may be uniquely determined (subject to certain constraints) [13], [15]. By amplitude and phase, we refer to the slowly varying, time-dependent complex quantity  $\tilde{\mathcal{E}}(t) = \sqrt{I(t)} \exp[i\phi(t)]$ . The delay stage in the correlator is scanned with a stepper motor, and exposure times are such that the signal from several hundred pulses is integrated each step. In all measurements, an aperture is used before the SHG-FROG apparatus to select only the on-axis portion of the beam. We employ several checks in all measurements to validate the results and eliminate systematic errors. The spectrum of the propagated fundamental (corrected for instrument response) is recorded and its autoconvolution is compared to the frequency marginal of the SHG-FROG measurement, thus correcting for the bandwidth limitations [16]. The same spectrum is also compared with the spectrum recovered by the SHG-FROG algorithm. We also make a second SHG-FROG measurement, letting the initially measured field propagate through 5 cm of BK-7 glass at low intensity. The information from this second measurement, along with the known dispersion of the BK-7, is used to remove the time ambiguity of the initial measurement.

Fig. 1 shows the evolution of the on-axis temporal field of an intense pulse as it propagates through fused silica. All fields are retrieved from SHG-FROG measurements. In Fig. 1(a), we present the intensity and phase of the input pulse. Plots (b) and (c) of this figure show the intensity and phase of the same pulse after having traveled through 1.27 cm and 2.54 cm of fused silica, respectively. In addition, plots (b) and (c) show the calculated intensity and phase using the measured field of Fig. 1(a) as an initial condition to the 1-D nonlinear Schrödinger equation:

$$\frac{\partial \tilde{\mathcal{E}}}{\partial z} + i \frac{k_o''}{2} \frac{\partial^2 \tilde{\mathcal{E}}}{\partial \tau^2} - i \frac{k_o n_2}{n_o} |\tilde{\mathcal{E}}|^2 \tilde{\mathcal{E}} = 0. \quad (1)$$

In this equation,  $\tilde{\mathcal{E}}(z, \tau)$  is the slowly varying complex amplitude of the field in the rest frame moving at the group velocity. The wave vector is  $k_o = 2\pi n_o / \lambda_o$ , with  $n_o$  being the linear index of refraction at the center wavelength  $\lambda_o$ . The GVD is determined by  $k_o''$ , which is the second derivative of  $k$  (with respect to frequency) evaluated at  $\lambda_o$ . The instantaneous nonlinear index of refraction is denoted by  $n_2$ , and the field is normalized such that  $|\tilde{\mathcal{E}}|^2 = I$  is the intensity in units of  $\text{W}/\text{cm}^2$ . Given the initial field of Fig. 1(a), we then solve (1) using a split-step technique [17], [18]. As can be seen

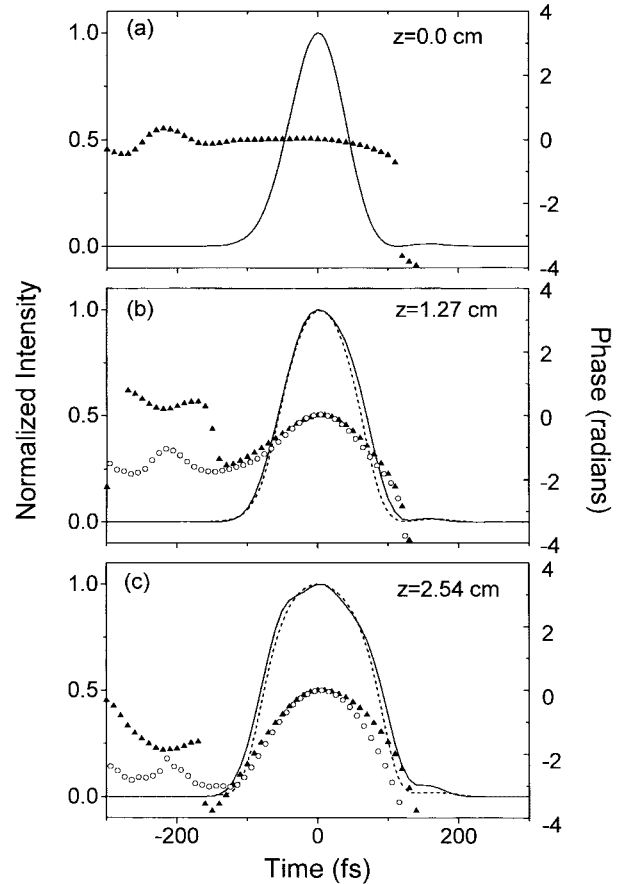


Fig. 1. Temporal field of an intense femtosecond pulse at propagation distances in fused silica of  $z = 0, 1.27,$  and  $2.54$  cm. The experimentally measured intensity (solid lines) and phase (solid triangles) are shown in all three plots. The calculated intensity (dashed lines) and phase (open circles) are also shown in plots (b) and (c).

in Fig. 1(b) and (c), good agreement exists between the measurement and the theory. Here we have taken the input peak intensity to be  $57 \text{ GW}/\text{cm}^2$ , which we calculate from the measured pulse energy, beam diameter (assumed Gaussian), and the temporal profile shown in Fig. 1(a). In addition, we use the values of  $n_o = 1.46$ ,  $\lambda_o = 800$  nm, and  $k_o'' = 360 \text{ fs}^2/\text{cm}$ . The value of  $n_2$  can then be used as a fitting parameter. For these measurements  $n_2 = 2.5 \times 10^{-16} \text{ cm}^2/\text{W}$  gives the best agreement between experiment and theory. This value of  $n_2$  is in good agreement with other recent measurements [19], [20]. These positive results give us confidence that the SHG-FROG technique can be applied to the more complicated propagation measurements presented in the later sections of this paper.

The use of (1) to model the experimental conditions is justified as long as the field is well approximated by a plane wave during its propagation. This is indeed the situation for the large diameter beam, which has a confocal parameter  $z_o = \pi n_o w_o^2 / \lambda_o$  of many tens of meters. The peak power of the pulses used in these measurements is near 10 GW. This power is many orders of magnitude greater than the critical power for self-focusing  $P_{\text{crit}} = (0.61 \lambda_o)^2 \pi / (8 n_o n_2)$  [7], which evaluates to  $P_{\text{crit}} = 2.6 \text{ MW}$  for fused silica at  $\lambda_o = 800$  nm. However, the self-focusing length,  $z_f = w_o \sqrt{n_o / (n_2 I)}$  [7], is

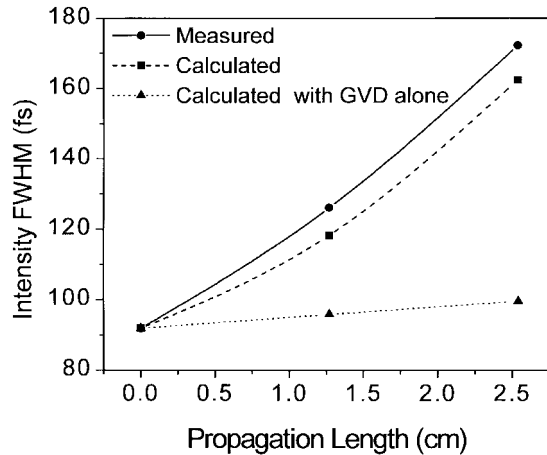


Fig. 2. Measured and calculated FWHM of the intensities of the fields presented in Fig. 1. All calculations use the measured field of Fig. 1(a) as an input.

still on the order of 50 cm, which is more than twenty times greater than the propagation length. The validity of this plane-wave approximation is further confirmed by comparing the results obtained from (1) with the results of a full 3-D model, which we present later in this paper. For the experimental conditions outlined above, both the 1-D and 3-D models give near-identical results.

To lowest order, (1) includes the effects of temporal self-phase modulation (SPM) and dispersion. During propagation in the regime of positive GVD ( $k_o'' > 0$ ) and positive  $n_2$ , one anticipates that both dispersion and temporal SPM will act to impose a predominantly positive chirp on the pulse. Although SPM by itself does not contribute to any temporal broadening, its combination with +GVD enhances the positive chirp and increases the broadening. Similar results have been observed in optical fibers where (1) also applies [21]. However, we believe the data of Fig. 1 provide the first amplitude and phase measurement detailing the interplay of +GVD and SPM in bulk propagation. The importance of the interplay of +GVD and SPM is further illustrated in Fig. 2, where we plot the full-width at half maximum (FWHM) of the measured and calculated intensities as a function of propagation length. In addition, we also plot the calculated FWHM for the case of  $n_2 = 0$  (GVD alone). As can be seen, with no nonlinearity and 2.5 cm of propagation, the pulse is predicted to broaden about 5 fs from the initial FWHM of 92 fs. However, the inclusion of the nonlinearity leads to dramatic broadening of nearly 80 fs for the same propagation length, resulting in a FWHM of  $\sim 170$  fs. The fact that the calculated FWHM is slightly less than the measured may be due to the inertial (Raman) response of the fused silica, which is not accounted for in (1).

### III. 3-D PROPAGATION

The addition of transverse dimensions to the problem of nonlinear femtosecond pulse propagation results in interesting and unexpected phenomena. For the case of +GVD and  $+n_2$ , the full spatio-temporal evolution of a femtosecond

pulse has been studied theoretically in some detail. It has been shown that the inclusion of diffraction and self-focusing can result in the situation where the pulse splits temporally [22]–[25]. We emphasize this in contrast to the 1-D situation presented in the previous section where pulse splitting is not observed. In fact, for Gaussian input pulses, (1) does not predict pulse splitting—even with higher intensities and greater propagation distances. Measurements of the spectrum of a self-focusing femtosecond pulse have implied that the pulse develops temporal substructure [26], [27], and intensity autocorrelation measurements by Ranka *et al.* [28] validate the predictions of pulse splitting in the time domain. However, these measurements lack full information about the amplitude and phase of the field. In order to provide a more complete picture of this complicated situation, we have recently used SHG-FROG to measure the complete on-axis temporal field of a self-focusing femtosecond pulse [29]. The full temporal field, as provided by the SHG-FROG measurement, gives a more complete picture of the dynamics, and should allow us to test the validity of the NLSE (and its variations) for describing nonlinear pulse propagation.

If we assume azimuthal symmetry, we can include the transverse dimension to the NLSE such that (1) takes the following form:

$$\frac{\partial \tilde{\mathcal{E}}}{\partial z} - \frac{i}{2k_o} \nabla_{\perp}^2 \tilde{\mathcal{E}} + \frac{ik_o''}{2} \frac{\partial^2 \tilde{\mathcal{E}}}{\partial \tau^2} - i \frac{k_o n_2}{n_o} |\tilde{\mathcal{E}}|^2 \tilde{\mathcal{E}} = 0. \quad (2)$$

The only difference between this equation and (1) is the radial Laplacian  $\nabla_{\perp}^2$ , and the additional radial dependence of the field  $\tilde{\mathcal{E}}(z, r, \tau)$ . Numerical solutions of (2) are performed, using the Crank–Nicholson method to compute the derivatives. For all simulations, we assume a real input field given by

$$\tilde{\mathcal{E}}(z=0, r, \tau) = \sqrt{I_o} \exp(-r^2/2r_o^2) \operatorname{sech}(\tau/\tau_o). \quad (3)$$

All parameters are the same as those used in the one-dimensional model of (1) along with  $n_2 = 2.5 \times 10^{-16}$  cm<sup>2</sup>/W. The input FWHM of the pulse of (3) is set at 70  $\mu$ m in the spatial domain and 90 fs in temporal domain. Sample theoretical results are shown in Fig. 3 where we present normalized intensity surface plots at three propagation distances in the fused silica. Fig. 3(a) is the input field as described by (3), with peak intensity of 87 GW/cm<sup>2</sup>. Fig. 3(b) and (c) are the intensity distributions at  $z = 2.0$  cm and  $z = 3.0$  cm, respectively. As can be seen, the field is initially focused both in space and time before it ultimately splits into two pulses along the temporal coordinate.

The evolution seen in Fig. 3 is summarized by Fig. 4, where we plot both the calculated on-axis ( $r = 0$ ) temporal FWHM of the pulse and the peak intensity. With reference to both Figs. 3 and 4(a), we see that as the pulse focuses spatially, its on-axis temporal width actually decreases by close to 50%. This phenomenon is the pulse sharpening first predicted and measured 30 years ago [30], [31]. Put simply, it is the result of the self-focusing induced transfer of off-axis energy toward the peak of the pulse. At about the position  $z = 1.75$  cm,

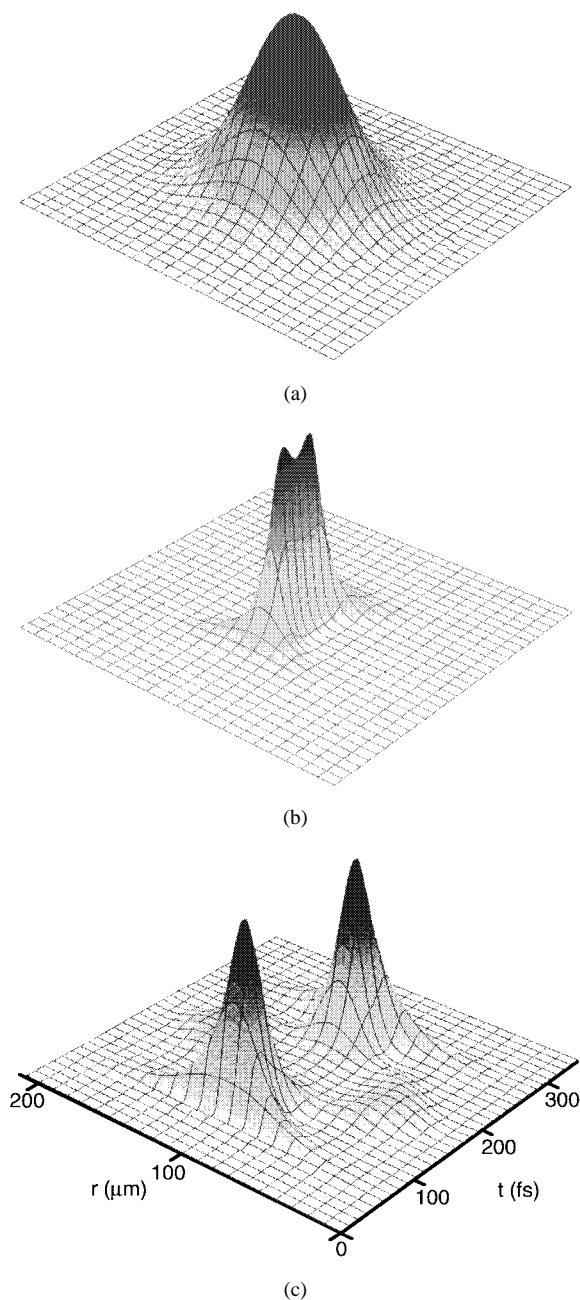


Fig. 3. Calculated intensity surface plots of a self-focusing femtosecond pulse at three different propagation lengths: (a) input; (b)  $z = 2.0$  cm; and (c)  $z = 3.0$  cm. The temporal and spatial scales on all plots are the same; however, the intensities have all been normalized by the peak value.

the pulse stops focusing temporally, and at  $z = 2.2$  cm the pulse is split to the extent that the FWHM of the two subpulses may be measured. It is at this point that we see the discontinuity in Fig. 4(a), as the individual split pulses each have FWHM on the order of 30 fs. These trends are mirrored in Fig. 4(b) where the on-axis peak intensity is plotted as a function of the same propagation distance. The  $15\times$  increase in intensity is primarily due to the strong spatial self-focusing rather than the reduction in pulsewidth (see also Fig. 3). It is at the position  $z = 1.95$  in Fig. 4(b) that two individual peaks are first recognizable and the discontinuity occurs in the figure.

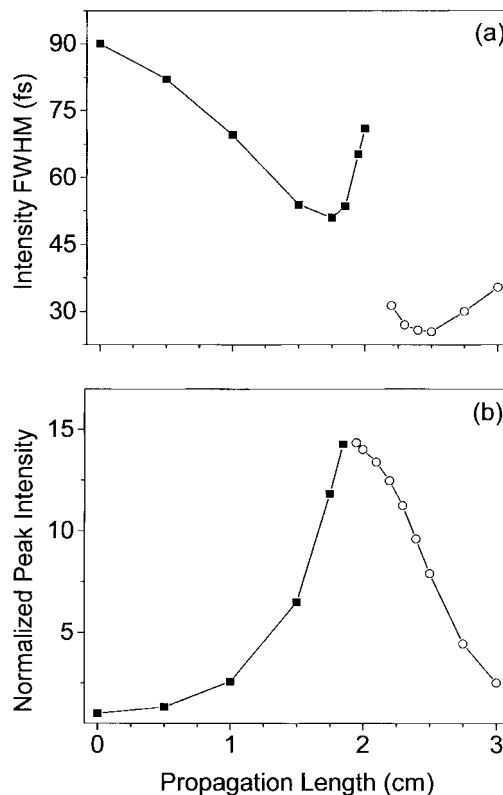


Fig. 4. (a) Calculated temporal FWHM and (b) peak intensity of a femtosecond pulse propagating in fused silica. The solid squares are for the pulse prior to splitting, while the open circles designate the pulse after splitting. The lines are meant only to guide the eye. See text for further details.

From a simple physical standpoint, we understand the process of pulse splitting as follows: Initially, strong self-focusing moves off-axis energy toward the peak of the pulse and compresses it in both space and time [30]. As the peak intensity increases, the process of SPM also increases, thereby generating new frequency components. The combination of the SPM-induced up-chirp and +GVD then act to push the energy away from  $\tau = 0$ , initiating the pulse splitting. As this process continues, the peak intensity drops, stopping the collapse at  $\tau = 0$ . However, off-axis energy continues to focus at  $\tau \neq 0$  such that two pulses are resolved [24].

#### A. Experimental Results at 800 nm

For the following measurements, the output from the same laser system described above is strongly attenuated and then focused with a 50-cm focal length lens to a spot size of  $70\text{-}\mu\text{m}$  FWHM at the entrance face of the fused silica sample. After propagation in the fused silica, the beam is allowed to diverge for  $\sim 75$  cm. The central 5%–10% of the beam is then selected with an aperture and used as input to the SHG-FROG apparatus described above. In contrast to the 1-D experiments described above, the peak power of the pulses used in these experiments is much lower—typically one to three times the critical power for self-focusing. However, both the self-focusing length  $z_f$  and the confocal parameter  $z_o$  are on the order of the propagation length, meaning that transverse changes in the beam may no longer be neglected.

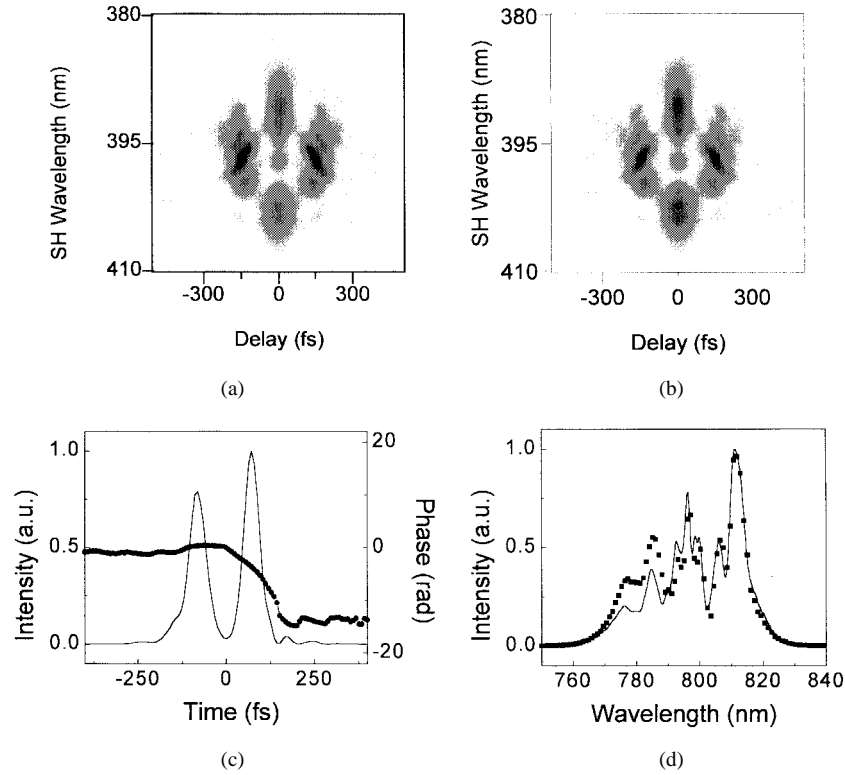


Fig. 5. SHG-FROG data of split pulse. (a) Measured and (b) recovered SHG-FROG traces. (c) Recovered intensity (line) and phase (points). (d) Recovered (points) and measured spectrum (line).

Experimental SHG-FROG data that demonstrates the predicted splitting is shown in Fig. 5. For this data, the length of the fused silica is 2.54 cm. The input pulse has a FWHM of 92 fs and a peak intensity of  $88 \text{ GW/cm}^2$ , meaning the peak power is  $1.9P_{\text{crit}}$ . It is worth noting the excellent agreement between the measured SHG-FROG trace of Fig. 5(a), and the retrieved SHG-FROG trace of Fig. 5(b). Such agreement is typical, indicating good convergence of the phase retrieval algorithm and boosting our confidence in the ability of SHG-FROG to characterize complicated pulses. The intensity and phase of the retrieved field are shown in Fig. 5(c), while Fig. 5(d) shows the recovered spectrum [Fourier transform of Fig. 5(c)] and the independently measured spectrum. Here again, we have good agreement, even with the complicated structure. As seen in Fig. 5(c) the near-Gaussian input pulse has completely split into two pulses having FWHM of roughly 50 fs. In contrast to the calculated splitting of Fig. 3, both the intensity and phase are asymmetric. It is believed that this asymmetry is due to nonlinear shock formation and space-time focusing [32], with cubic temporal phase variations on the initial field playing a lesser role [33]. These mechanisms are explored in a future publication [34]. The Raman response of the fused silica is investigated as a possible source of asymmetry in a later section of this paper. Although the intensity of the self-focused field approaches the  $\text{TW/cm}^2$  level, we see no intensity-dependent loss which would indicate multiphoton absorption or ionization. Furthermore, no visible signs of permanent damage are observed in the fused silica.

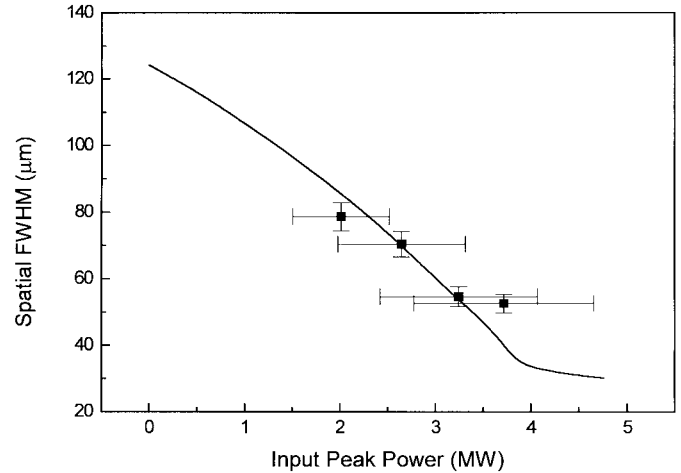


Fig. 6. Measured spatial FWHM of beam size as a function of peak power (points). The solid curve is the calculated beam size assuming a Gaussian spatial profile for the input beam.

Measurements illustrating changes in the spatial profile of the beam are presented in Fig. 6. Here, we present the measured beam diameter at the exit face of a 3.0-cm fused silica sample at four different input powers corresponding to various degrees of pulse splitting. SHG-FROG measurements of the temporal field are also made at these same input powers, allowing us to monitor the degree of temporal splitting. The time-domain results are similar to previously published data that show the intensity dependence of the pulse splitting [29]. The beam diameters shown in Fig. 6 are obtained by imaging

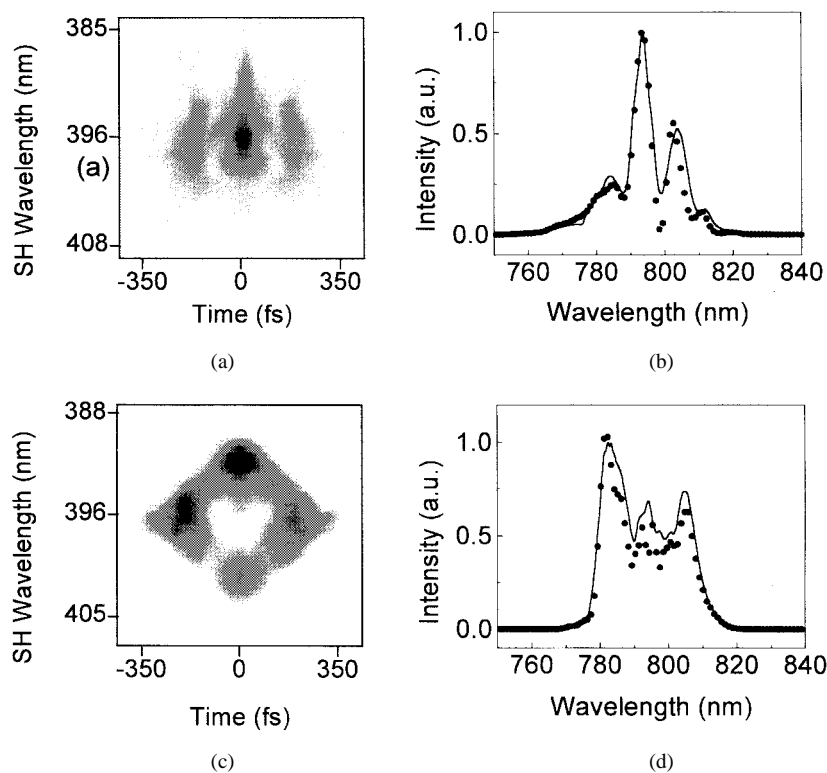


Fig. 7. Measured SHG-FROG traces for (a) down-chirped and (c) up-chirped input pulses for a peak intensity of  $57 \text{ GW/cm}^2$ . The corresponding measured spectra (line) and retrieved spectra (points) are shown in (b) and (d), respectively.

the exit face of the fused silica sample onto a charge-coupled device (CCD) camera with a magnification of  $+2.8$ . The two points at the lowest powers correspond to pulses that have broadened temporally, but have not yet split. At the third point, the pulse is partially split, such that the intensity between the two pulses drops to half the peak value. At the highest peak power, the pulse is completely split—similar to Fig. 5(c). The solid line in Fig. 6 shows the calculated beam diameter assuming the input field of Fig. 3(a). This calculated beam diameter is obtained by integrating over the temporal dimension of intensity plots similar to those presented in Fig. 3. Both the theoretical and experimental results demonstrate that the spot size approaches a constant value at powers where pulse splitting occurs. The measurements indicate that this regime occurs at lower powers than predicted by the theory. Although, as seen in Fig. 6, the error in the measured power is on the order of 25% due to uncertainties in the measured pulse energy and the temporal profile of the pulse. In addition, the measured spot size is never as small as the calculated value. This discrepancy may arise from spatial profile deviations of the actual beam from an ideal Gaussian.

In previous measurements, we reported on the intensity dependence of the pulse splitting [29]. Here, we provide more detailed measurements describing the influence of the chirp of the input pulse on the propagation process. It is possible to create a predominantly linearly chirped pulse by lengthening or shortening the grating compressor of our chirped pulse amplification system. We can then use FROG to accurately characterize the chirped pulse before and after propagation through the fused silica sample. The up-chirped pulse for

these measurements has a temporal FWHM of 147 fs, and the down-chirped pulse has a temporal FWHM of 153 fs. Each of the chirped input pulses is propagated through the fused silica sample at two different peak intensities. The lower peak intensity values are 45 and  $49 \text{ GW/cm}^2$  for the up- and down-chirped pulses, respectively. The higher input peak intensity is  $57 \text{ GW/cm}^2$  for both up- and down-chirped pulses.

Fig. 7 shows the measured SHG-FROG traces obtained with chirped input pulses in each of the higher intensity cases. In addition, both the retrieved and independently measured spectra are plotted for comparison. The characteristic shape of the SHG-FROG trace for pulse splitting with a down-chirped input pulse [Fig. 7(a)] is very different than when the input pulse is up-chirped [Fig. 7(c)]. An up-chirped input pulse leads to SHG-FROG traces which are largely diamond shaped, with decreasing intensity in the center of the trace for greater splitting. A down-chirped input pulse, on the other hand, maintains a significant intensity in the center of the trace. Fig. 8 shows the retrieved time and spectral domain intensity and phase for each of the four input pulse cases. At higher peak powers, the amount of pulse splitting and spectral modulation increases. When an initially down-chirped pulse [Fig. 8(a) and (b)] splits temporally, the resulting pulses are about two-times narrower than those produced from the splitting of an up-chirped pulse [Fig. 8(c) and (d)]. In addition, the spectra in Fig. 8(e) and (f) (down-chirped input) are narrower than the spectra of Fig. 8(g) and (h) (up-chirped input). A simple explanation for these observations arises from the fact that both  $+GVD$  and  $SPM$  (with  $+n_2$ ) act to produce positive, linear chirp over the central region

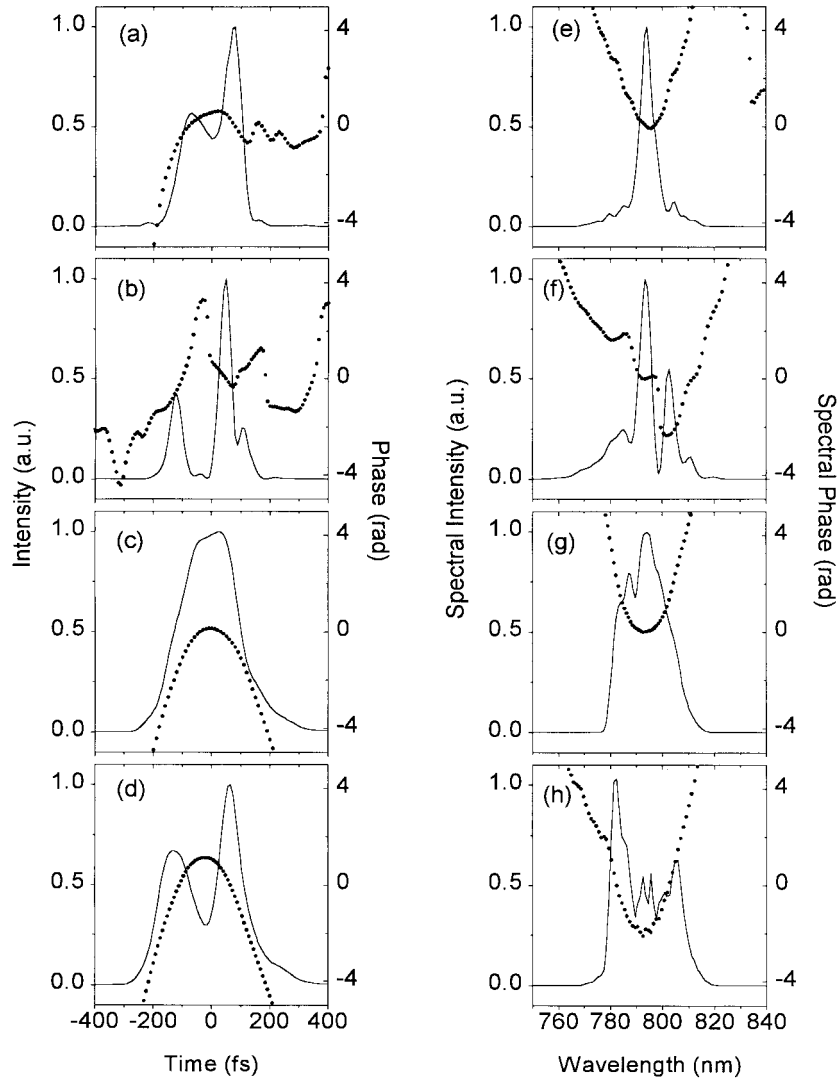


Fig. 8. Retrieved fields from SHG-FROG. (a)–(d) Temporal intensity (line) and phase (points); (e)–(h) associated spectral intensity (lines) and phase (points). (a), (b) correspond to down-chirped input at 49 and 57 GW/cm<sup>2</sup>. (c), (d) correspond to up-chirped input at 45 and 57 GW/cm<sup>2</sup>.

of the pulse. Thus, an initial up-chirp on the pulse acts as a head start to the propagation induced up-chirp, resulting in broader pulses. An initial down-chirp, however, acts to negate the propagation induced up-chirp, yielding shorter split pulses at the output. The narrower (and deeply modulated) spectrum seen with the down-chirped input can be interpreted as destructive interference between existing frequencies and new frequencies created by SPM. Note also that the spectral phase after propagation for all four cases has an overall concave-up curvature, regardless of the sign of the chirp of the input pulse. This phase curvature implies an up-chirp across the total split field such that the leading pulse is spectrally redshifted compared to the trailing pulse. This up-chirp is due to the combined effects of positive GVD and SPM in the regime of  $+n_2$ , as discussed earlier.

### B. Experimental Results at 1200 nm

We also present preliminary measurements using the output of a femtosecond optical parametric amplifier (OPA). The OPA

used is similar to that described by Yakovlev [35], consisting of single-pass amplification of infrared continuum in a 4-mm BBO crystal (Type-I phase matching). When pumped at 800 nm, the OPA produces signal fields with wavelengths in the range of 1100–1400 nm. This is an interesting regime in which to study propagation because these wavelengths are predominantly used for optical communications in fused silica fibers. In addition, in this wavelength range, the GVD in fused silica decreases in magnitude and then changes sign from positive to negative near 1250 nm, while  $n_2$  remains approximately constant. With  $-GVD$  (anomalous dispersion) and  $+n_2$ , it has been predicted that spatio-temporal solitons can propagate—provided  $+n_2$  saturates or there exists a higher order intensity-dependent term with opposite sign [36]. From a practical point of view, such 3-D solitons could have important implications for optical communications and all-optical switching [37], [5].

To insure good beam quality, the output of the OPA is spatially filtered and recollimated before being focused onto

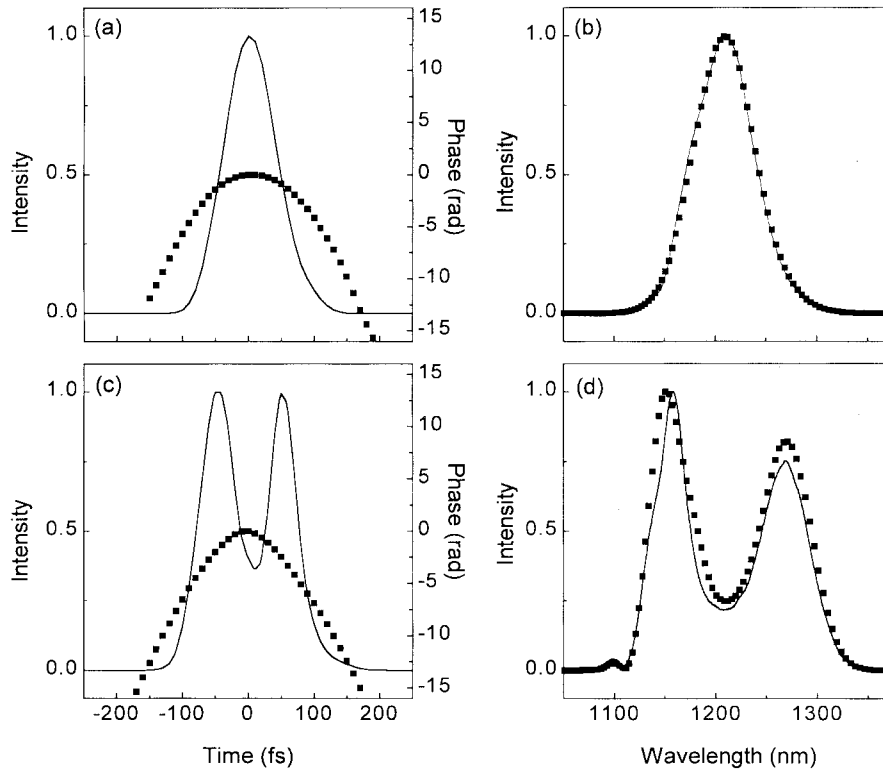


Fig. 9. Measured fields at 1200 nm. (a) Intensity (line) and phase (points) of input field. (b) Corresponding measured spectrum (line) and spectrum retrieved from SHG-FROG (points). Plots (c) and (d) are the same as (a) and (b), except the pulse has traveled through 3.0 cm of fused silica.

the entrance face of the fused silica sample in the same manner described above. Beam parameters are approximately the same as those used at 800 nm, so that qualitative comparisons can be made between the two situations. Results at the wavelength of 1.2  $\mu\text{m}$  are shown in Fig. 9. In this figure, we show the temporal intensity and phase before and after propagation through the same 3.0-cm fused silica sample used for measurements at 800 nm. The corresponding spectra recovered from SHG-FROG, and the independently measured spectra are also shown. Here, again we see excellent agreement between the recovered and measured spectra. The input field of Fig. 9(a) has a FWHM duration of 92 fs, but the large negative curvature of the phase indicates the existence of significant linear up-chirp. Indeed, the time-bandwidth product is three times the transform limit, implying 30-fs pulses could be generated if the up-chirp were properly compensated. After propagation through the fused silica, we see in Fig. 9(c) that the pulse begins to split. The input peak power in this case is 9 MW, or  $1.5P_{\text{crit}}$ , assuming the value of  $n_2$  is the same at both 800 and 1200 nm. With a 10% increase in the power above 9 MW, we observe rapid spectral broadening and continuum generation. From (2), one would expect splitting to be less pronounced in this regime because of the decrease in the GVD. Indeed, no splitting is predicted in numerical solutions of (2) when a value of  $k''_0 = 60 \text{ fs}^2/\text{cm}$  is used. These results, together with the results of recent simulations [38], indicate that the third-order dispersion plays an important role in pulse splitting in this wavelength regime.

#### IV. 3-D PROPAGATION INCLUDING THE RAMAN RESPONSE

It is interesting to explore the possible sources of asymmetry observed in the experimental data presented in the previous section and in our previous work [29]. As written (2) is symmetric in time and space, such that for a symmetric input the output is also symmetric. An obvious source of asymmetry is an initial asymmetry of the input pulse—in amplitude and phase of either the temporal or spatial dimensions. Furthermore, the addition of third-order dispersion to (2) creates temporal asymmetries. Another possibility is a noninstantaneous nonlinearity such as Raman scattering, which is discussed here in further detail. It is well known that the nonlinear susceptibility of fused silica is comprised of both a near-instantaneous electronic response and a slower nuclear response [39]. The slower response, also called the Raman response, is due to nuclear vibrations excited by the optically induced (fast) perturbation of the electronic structure. The characteristic Raman response time is on the order of 50–100 fs and can comprise up to 20% of the total nonlinear response [39]–[41].

The Raman contribution to the refractive index can be modeled by replacing the nonlinear term in (2) with the following:

$$n_2|\tilde{\mathcal{E}}(\tau)|^2 \rightarrow n_2 \left\{ (1 - \alpha)|\tilde{\mathcal{E}}(\tau)|^2 + \alpha \int_{-\infty}^{\tau} f(\tau - t')|\tilde{\mathcal{E}}(t')|^2 dt' \right\}. \quad (4)$$

In this equation,  $\alpha$  is the fraction of the nonlinearity resulting

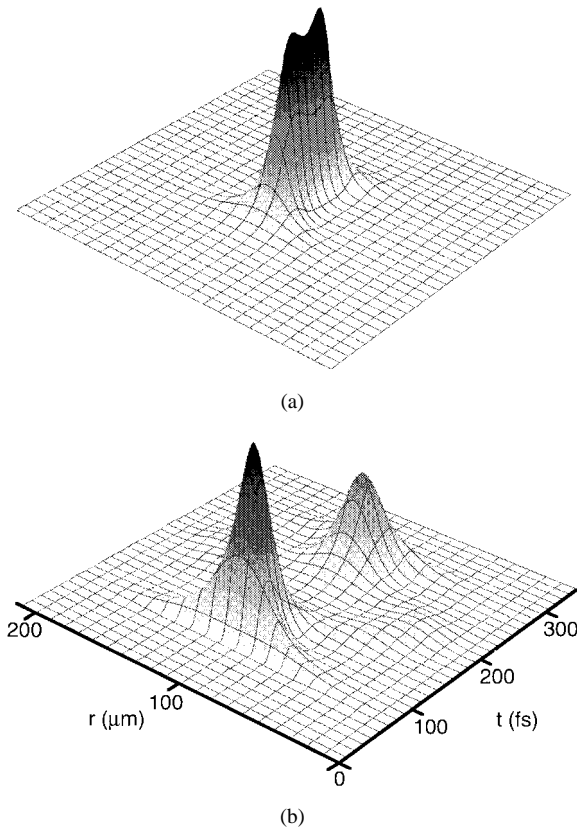


Fig. 10. Calculated intensity surface plots of a self-focusing femtosecond pulse with the inclusion of the Raman response: (a)  $z = 2.0$  cm and (b)  $z = 3.0$  cm. The temporal and spatial scales on all plots are the same; however, the intensities have been normalized by the peak value.

from the Raman contribution and  $f(\tau - t')$  is the normalized Raman response function, which we approximate by [41]

$$f(t) = \frac{1 + (\omega_r \tau_r)^2}{\omega_r \tau_r^2} \exp\left\{-\frac{t}{\tau_r}\right\} \sin(\omega_r t). \quad (5)$$

In all numerical simulations, we use  $\alpha = 0.18$ ,  $\tau_r = 50$  fs and the dimensionless quantity  $\omega_r \tau_r = 4.2$ .

Intensity surface plots at propagation distances of  $z = 2.0$  cm and  $z = 3.0$  cm are shown in Fig. 10. The input pulse for these simulations is the same as shown in Fig. 3(a). The principle change due to the inclusion of the Raman effect is the asymmetry between the leading and trailing pulses. As can be seen, at the position  $z = 3.0$  cm, the leading pulse has almost twice the peak intensity of the trailing pulse. The increase of the leading pulse at the expense of the trailing pulse can be understood simply in terms of Raman gain. The response function of (5) is the time-domain representation of the more common frequency-domain picture of stimulated Raman scattering, whereby red-shifted frequency components are amplified at the expense of the blue-shifted components. Since in this case +GVD and SPM move the red components ahead of the blue components, it follows that the leading pulse should be larger because of the preferential Raman gain. Therefore, we conclude that Raman scattering is not the direct source of the observed asymmetry in the intensities of the fully split pulses in Figs. 5 and 8.

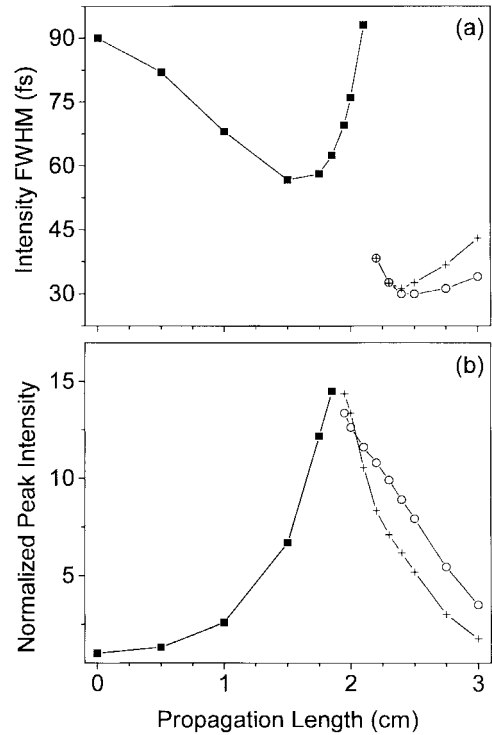


Fig. 11. Same as Fig. 4, but with the inclusion of the Raman response of the medium. The solid squares are for the pulse prior to splitting. After splitting, the open circles designate the leading pulse, while the crosses are for the trailing pulse. The lines are meant only to guide the eye. See text for further details.

Details of the evolution of the on-axis temporal profile and the peak intensity of the pulse with the Raman term included are shown in Fig. 11. Similar to the previous case with no Raman contribution, during the first 1.5 cm of propagation the on-axis temporal FWHM decreases by about 30%. The pulse then starts to broaden, but it is not until the position  $z = 1.95$  cm that two peaks begin separating out of the single pulse. The separation of these two nascent pulses continues until  $z = 2.2$  cm, which is the point where each of the two pulses can be characterized by its own FWHM. This is the point at which the line in Fig. 11(a) bifurcates, and the individual FWHM of the two pulses are tracked until  $z = 3.0$  cm. In the last 0.5 cm of propagation the individual pulses start to broaden, with the trailing pulse broadening more rapidly.

The peak intensity of the field (normalized by the peak input intensity) as shown in Fig. 11(b) complements the temporal behavior. The temporal compression seen in Fig. 11(a) is accompanied by strong spatial compression which results in a ten fold increase in the peak intensity after a few centimeters of propagation. As noted above, at the position  $z = 1.95$  cm two distinct peaks are resolved. It is at this point that the curve of Fig. 11(b) bifurcates and the individual peak intensities are tracked independently. Once splitting starts, it is evident that the peak intensities of both pulses fall rapidly. An interesting point seen in Fig. 11(b) is that when the pulse first begins to split, the trailing peak has a higher intensity than the leading peak. At about  $z = 2.1$  cm, this trend reverses and the leading pulse maintains a higher peak intensity.

## V. CONCLUSION

We have shown that FROG can be a useful tool in studying the nonlinear propagation of intense femtosecond pulses in nonlinear, dispersive media. In situations that can be modeled with the 1-D NLSE, we obtain excellent agreement between the measured and calculated electric fields, and we observe rapid temporal broadening from the combined effects of GVD and SPM. In situations where the full 3-D nature of the field must be considered, we have measured the splitting of an input pulse into subpulses that are almost two times shorter than the input. This splitting is not generally symmetric, and we have presented calculations that indicate that Raman scattering is not the direct source of the observed asymmetry. In addition, we have made measurements that illustrate the effect of input linear chirp on the pulse splitting. Finally, we have presented data for propagation of femtosecond pulses at 1200 nm, demonstrating that these pulses undergo temporal splitting when self-focused in fused silica. At 1200 nm, numerical simulations indicate that third-order dispersion must be taken into consideration to fully explain the splitting.

## ACKNOWLEDGMENT

The authors thank S. Blair for his helpful comments.

## REFERENCES

- [1] J.-C. Diels and W. Rudolph, *Ultrashort Laser Pulse Phenomenon: Fundamentals, Techniques and Applications on a Femtosecond Time Scale*. Boston, MA: Academic, 1996.
- [2] X. M. Zhao, J.-C. Diels, C. Y. Wang, and J. Elizondro, "Femtosecond ultraviolet laser pulse induced electrical discharges in gases," *IEEE J. Quantum Electron.*, vol. 31, pp. 599–612, 1995.
- [3] A. Braun, G. Korn, X. Liu, D. Du, J. Squier, and G. Mourou, "Self-channeling of high-peak-power femtosecond laser pulses in air," *Opt. Lett.*, vol. 20, pp. 73–75, 1995.
- [4] E. T. J. Nibbering, P. F. Curley, G. Grillon, B. S. Prade, M. A. Franco, F. Salin, and A. Mysyrowicz, "Conical emission from self-guided femtosecond pulses in air," *Opt. Lett.*, vol. 21, pp. 62–64, 1996.
- [5] R. McLeod, K. Wagner, and S. Blair, "(3 + 1)-dimensional optical soliton dragging logic," *Phys. Rev. A*, vol. 52, pp. 3254–3278, 1995.
- [6] P. Gibbon and E. Förster, "Short-pulse laser-plasma interactions," *Plasma Phys. Control. Fusion*, vol. 38, pp. 769–793, 1996.
- [7] R. W. Boyd, *Nonlinear Optics*. San Diego, CA: Academic, 1992.
- [8] R. R. Alfano, Ed., *The Supercontinuum Laser Source*. New York: Springer-Verlag, 1989.
- [9] Q. Feng, J. V. Moloney, A. C. Newell, E. M. Wright, K. Cook, P. K. Kennedy, D. X. Hammer, B. A. Rockwell, and C. R. Thompson, "Theory and simulation on the threshold of water breakdown induced by focused ultrashort laser pulses," *IEEE J. Quantum Electron.*, vol. 33, pp. 127–137, Feb. 1997.
- [10] G. Fibich and G. C. Papanicolaou, "Self-focusing in the presence of small time dispersion and nonparaxiality," *Opt. Lett.*, vol. 22, pp. 1379–1381, 1997.
- [11] D. Anderson and M. Lisak, "Nonlinear asymmetric self-phase modulation and self-steepening of pulses in long optical waveguides," *Phys. Rev. A*, vol. 27, pp. 1393–1398, 1983.
- [12] D. J. Kane and R. Trebino, "Single-shot measurement of the intensity and phase of an arbitrary ultrashort pulse by using frequency-resolved optical gating," *Opt. Lett.*, vol. 18, pp. 823–825, 1993.
- [13] R. Trebino and D. J. Kane, "Using phase retrieval to measure the intensity and phase of ultrashort pulses: Frequency-resolved optical gating," *J. Opt. Soc. Amer. A*, vol. 10, pp. 1101–1111, 1993.
- [14] K. W. DeLong, R. Trebino, and D. J. Kane, "Comparison of ultrashort-pulse frequency-resolved-optical-gating traces for three common beam geometries," *J. Opt. Soc. Amer. B*, vol. 11, pp. 1595–1608, 1994.
- [15] K. W. DeLong, D. N. Fittinghoff, R. Trebino, B. Kohler, and K. Wilson, "Pulse retrieval in frequency-resolved optical gating based on the method of generalized projections," *Opt. Lett.*, vol. 19, pp. 2152–2154, 1994.
- [16] G. Taft, A. Rundquist, M. M. Murnane, I. P. Christov, H. C. Kapteyn, K. W. DeLong, D. N. Fittinghoff, M. A. Krumbügel, J. N. Sweetser, and R. Trebino, "Measurement of 10-fs laser pulses," *IEEE J. Select. Topics Quantum Electron.*, vol. 2, pp. 575–585, 1996.
- [17] G. P. Agrawal, *Nonlinear Fiber Optics*. San Diego, CA: Academic, 1989.
- [18] E. T. J. Nibbering, P. F. Curley, G. Grillon, B. S. Prade, M. A. Franco, F. Salin, and A. Mysyrowicz, "Spectral determination of the amplitude and phase of intense ultrashort optical pulses," *J. Opt. Soc. Amer. B*, vol. 13, pp. 317–329, 1996.
- [19] E. T. J. Nibbering, M. A. Franco, B. S. Prade, G. Grillon, C. LeBlanc, and A. Mysyrowicz, "Measurement of the nonlinear refractive index of transparent materials by spectral analysis after nonlinear propagation," *Opt. Commun.*, vol. 119, p. 479, 1995.
- [20] A. J. Taylor, G. Rodriguez, and T. S. Clement, "Determination of  $n_2$  by direct measurement of the optical phase," *Opt. Lett.*, vol. 21, pp. 1812–1814, 1996.
- [21] H. Nakatsuka, D. Grischkowsky, and A. C. Balant, "Nonlinear picosecond-pulse propagation through optical fibers with positive group velocity dispersion," *Phys. Rev. Lett.*, vol. 47, pp. 910–913, 1981.
- [22] N. A. Zharova, A. G. Litvak, T. A. Petrova, A. M. Sergeev, and A. D. Yanukovskii, "Multiple fractionation of wave structures in a nonlinear medium," *J. Experimental Theoretical Phys. Lett.*, vol. 44, pp. 13–17, 1986.
- [23] P. Chernev and V. Petrov, "Self-focusing of light pulses in the presence of normal group-velocity dispersion," *Opt. Lett.*, vol. 17, pp. 172–174, 1992.
- [24] J. E. Rothenberg, "Pulse splitting during self-focusing in normally dispersive media," *Opt. Lett.*, vol. 17, pp. 583–585, 1992.
- [25] J. T. Manassah and B. Gross, "Self-focusing of  $(3 + 1) - d$  femtosecond pulses in nonlinear Kerr media," *Laser Phys.*, vol. 6, pp. 563–578, 1996.
- [26] D. Strickland and P. B. Corkum, "Short pulse self-focusing," in *Proc. SPIE in Short-Pulse High-Intensity Lasers and Applications*, H. A. Baldis, Ed., 1991, vol. 1413, pp. 54–58.
- [27] ———, "Resistance of short pulses to self-focusing," *J. Opt. Soc. Amer. B*, vol. 11, pp. 492–497, 1994.
- [28] J. K. Ranka, R. W. Schirmer, and A. L. Gaeta, "Observation of pulse splitting in nonlinear dispersive media," *Phys. Rev. Lett.*, vol. 77, pp. 3783–3786, 1996.
- [29] S. A. Diddams, H. K. Eaton, A. A. Zozulya, and T. S. Clement, "Amplitude and phase measurements of femtosecond pulse splitting in nonlinear dispersive media," *Opt. Lett.*, vol. 23, pp. 379–381, 1998.
- [30] J. H. Marburger and W. G. Wagner, "Self-focusing as a pulse sharpening mechanism," *IEEE J. Quantum Electron.*, vol. QE-3, p. 415, 1967.
- [31] G. L. McAllister, J. H. Marburger, and L. G. DeShazer, "Observation of optical pulse shaping by the self-focusing effects," *Phys. Rev. Lett.*, vol. 21, pp. 1648–1649, 1968.
- [32] J. E. Rothenberg, "Space-time focusing: Breakdown of the slowly varying envelope approximation in the self-focusing of femtosecond pulses," *Opt. Lett.*, vol. 17, pp. 1340–1342, 1992.
- [33] J. K. Ranka and A. L. Gaeta, "Nonlinear dynamics of the self-focusing of ultrashort pulses," presented at Ultrafast Optics 1997, Monterrey, CA, paper MB-3.
- [34] A. A. Zozulya, S. A. Diddams, and T. S. Clement, "Numerical investigations of nonlinear femtosecond pulse propagation with the inclusion of Raman, shock and third-order phase effects," *Phys. Rev. A*, submitted for publication.
- [35] V. V. Yakovlev, B. Kohler, and K. R. Wilson, "Broadly tunable 30-fs pulses produced by optical parametric amplification," *Opt. Lett.*, vol. 19, pp. 2000–2002, 1994.
- [36] Y. Silberberg, "Collapse of optical pulses," *Opt. Lett.*, vol. 15, pp. 1282–1284, 1990.
- [37] D. E. Edmundson and R. H. Enns, "Robust bistable light bullets," *Opt. Lett.*, vol. 17, pp. 586–588, 1992.
- [38] M. Trippenbach and Y. B. Band, "Dynamics of short-pulse splitting in dispersive nonlinear media," *Phys. Rev. A*, vol. 56, pp. 4242–4253, 1997.
- [39] R. Hellwarth, J. Cherlow, and T.-T. Yang, "Origin and frequency dependence of nonlinear optical susceptibilities in glass," *Phys. Rev. B*, vol. 11, pp. 964–967, 1975.
- [40] R. H. Stolen, J. P. Gordon, W. J. Tomlinson, and H. A. Haus, "Raman response function of silica core fibers," *J. Opt. Soc. Amer. B*, vol. 6, pp. 1159–1166, 1989.
- [41] R. H. Stolen and W. J. Tomlinson, "Effect of the Raman part of the nonlinear refractive index on propagation of ultrashort optical pulses in fibers," *J. Opt. Soc. Amer. B*, vol. 9, pp. 565–573, 1992.



**Scott A. Diddams** received the B.A. degree in physics from Bethel College, St. Paul, MN, in 1989, and the Ph.D. degree in optical science from the University of New Mexico, Albuquerque, NM, in 1996.

While at the University of New Mexico, he was a Graduate Fellow of the Center for Advanced Studies of the Department of Physics and Astronomy. Currently, he is a Post-Doctoral Research Associate at JILA, University of Colorado. His research interests include the generation, measurement and application of femtosecond laser pulses.



**Hilary K. Eaton** received the B.S. degree in chemistry from Furman University, Greenville, SC, in 1993, and is working toward the Ph.D. degree in physical chemistry at the University of Colorado, Boulder.



**Alex A. Zozulya** received the B.Sc. degree in physics from Moscow Engineering Physical Institute in 1978 and the Ph.D. degree in theoretical and mathematical physics from Lebedev Physics Institute of the Academy of Sciences of the U.S.S.R., in 1984.

His main research interests include plasma physics, photorefractive nonlinear optics, spatio-temporal solitons, propagation of ultrashort pulses, and atom optics.



**Tracy S. Clement** (S'89–M'92) received the Ph.D. degree in electrical engineering from Rice University in 1993. Her Ph.D. research involved developing and studying short wavelength (XUV and VUV) lasers and ultrashort pulse laser systems.

Since 1995, she has been working at JILA, where she is a staff Physicist with the National Institutes of Standards and Technology (NIST) and an Assistant Professor Adjoint in the Department of Physics at the University of Colorado, Boulder. From 1993 to 1995, she was a Director's Post-Doctoral Fellow at Los Alamos National Laboratory, Los Alamos, NM. Her current research interests are in ultrafast laser systems, nonlinear optics, and high-intensity light-material interactions.